J Biol Inorg Chem (2014) 19:787–803
DOI 10.1007/s00775-014-1110-0

ORIGINAL PAPER

Insights into the mechanisms underlying the antiproliferative potential of a Co(II) coordination compound bearing 1,10-phenanthroline-5,6-dione: DNA and protein interaction studies

Daniel V. Luís · Joana Silva · Ana Isabel Tomaz · Rodrigo F. M. de Almeida · Miguel Larguinho · Pedro V. Baptista · Luísa M. D. R. S. Martins · Telma F. S. Silva · Pedro M. Borralho · Cecília M. P. Rodrigues · António S. Rodrigues · Armando J. L. Pombeiro · Alexandra R. Fernandes

Received: 2 October 2013 / Accepted: 13 January 2014 / Published online: 31 January 2014

Abstract The very high antiproliferative activity of $[Co(Cl)(H_2O)(phendione)_2][BF_4]$ (phendione is 1,10-phenanthroline-5,6-dione) against three human tumor cell lines (half-maximal inhibitory concentration below 1 μM) and its slight selectivity for the colorectal tumor cell line compared with healthy human fibroblasts led us to explore the mechanisms of action underlying this promising antitumor potential. As previously shown by our group, this complex induces cell cycle arrest in S phase and subsequent cell death by apoptosis and it also reduces the expression of proteins typically upregulated in tumors. In the present work, we demonstrate that $[Co(Cl)(phendione)_2(H_2O)][BF_4]$ (1) does not reduce the viability of nontumorigenic breast epithelial cells by more than 85 % at 1 μM, (2) promotes the upregulation of proapoptotic Bax and cell-cycle-related p21, and (3) induces release of lactate dehydrogenase, which is partially reversed by ursodeoxycholic acid. DNA interaction studies were performed to uncover the genotoxicity of the complex and demonstrate that even though it displays K_b (± standard error of the mean) of $(3.48 \pm 0.03) \times 10^5\ M^{-1}$ and is able to produce double-strand breaks in a concentration-dependent manner, it does not exert any clastogenic effect ex vivo, ruling out DNA as a major cellular target for the complex. Steady-state and time-resolved fluorescence spectroscopy studies are indicative of a strong and specific interaction of the complex with human serum albumin, involving one binding site, at a distance of approximately 1.5 nm for the Trp214 indole side chain with log $K_b \sim 4.7$, thus suggesting that this complex can be efficiently transported by albumin in the blood plasma.

Keywords Cobalt · 1,10-Phenanthroline-5,6-dione · Apoptosis · DNA cleavage · Human serum albumin

D.V. Luís and J. Silva contributed equally to this work.

Electronic supplementary material The online version of this article (doi:10.1007/s00775-014-1110-0) contains supplementary material, which is available to authorized users.

D. V. Luís · J. Silva · M. Larguinho · P. V. Baptista · A. R. Fernandes (✉)
Departamento Ciências da Vida,
Faculdade de Ciências e Tecnologia,
Universidade Nova de Lisboa,
2829-516 Caparica, Portugal
e-mail: ma.fernandes@fct.unl.pt

A. I. Tomaz
Centro de Ciências Moleculares e Materiais,
Faculdade de Ciências, Universidade de Lisboa,
Campo Grande, 1749-016 Lisbon, Portugal

R. F. M. de Almeida
Centro de Química e Bioquímica,
Departamento de Química e Bioquímica,
Faculdade de Ciências, Universidade de Lisboa,
1749-016 Lisbon, Portugal

L. M. D. R. S. Martins · T. F. S. Silva · A. J. L. Pombeiro · A. R. Fernandes
Centro de Química Estrutural, Complexo I,
Instituto Superior Técnico, Universidade de Lisboa,
Lisbon, Portugal

L. M. D. R. S. Martins
Area Departamental de Engenharia Química, ISEL,
Lisbon, Portugal

P. M. Borralho · C. M. P. Rodrigues
Departamento de Bioquímica e Biologia Humana, Faculdade de Farmácia, Universidade de Lisboa, Lisbon, Portugal

Introduction

The discovery of the antitumor activity of cisplatin, which has been used in clinical practice as a chemotherapeutic agent since 1978 [1], led to increasing interest in metal complexes regarding their potential application in cancer treatment. Metal complexes offer the advantage of being very versatile molecules owing to the variety of intrinsic characteristics of both metal centers and ligands, making possible the design of complexes with a wide range of reactional properties, as discussed by Meggers [2]. Metal centers are prone to participate in nucleophilic substitution reactions owing to their cationic nature. Since both amino acids and nucleotides are able to act as nucleophiles [3], proteins and nucleic acids are important cellular targets for metal complexes. Indeed, the antitumor effect of platinum complexes is generally accepted to result from their reactivity towards DNA [4]. Nucleophilic substitution reactions result in the formation of DNA adducts or either intramolecular or intermolecular cross-linking, i.e., covalent interactions. In contrast, the presence of polycyclic aromatic ligands favors the establishment of three possible modes of noncovalent interaction with DNA, namely, groove binding, intercalation, and insertion [5]. Some metal complexes can also participate in nucleic acid cleavage, acting as artificial metallonucleases by catalyzing either direct hydrolysis [6] or oxidative cleavage by induction of reactive oxygen species (ROS) [7]. Transition metal complexes using 1,10-phenanthroline as ligands are capable of selectively binding DNA through intercalation [8–13]. Copper complexes of 1,10-phenanthroline and its derivatives are known to bind to DNA and cleave it in the presence of reducing agents, such as ascorbic acid [14–17]. Traditional anticancer drugs that target DNA make use of the fact that malignant cells divide rapidly. A drawback of this strategy is that rapidly dividing healthy cells are also affected, causing severe toxic side effects [18]. Worthy of note, before reaching the cell nucleus and being able to bind DNA in vivo, metal complexes may be able to interact with blood plasma proteins and/or with other cytoplasmic proteins, regardless of the administration route [19–21]. Indeed, cisplatin is vulnerable to attack by proteins found in the blood plasma, particularly those containing thiol groups, such as human serum albumin (HSA), and studies have shown that 1 day after cisplatin administration, 65–98 % of total cisplatin is bound [19]. Binding to plasma proteins is recognized as a crucial step in accessing the bioavailability of metal complexes [21], and reporting on plasma protein binding is now an FDA requirement in screening potential therapeutic agents [22]. HSA is the most abundant protein in plasma (approximately 60 % of total plasma protein) and, among its many functions, it stands out as the most important nonspecific transporter protein in the circulatory system, with a crucial effect on drug distribution and pharmacokinetics [23]. Albumin binding can increase the solubility of the prospective drug, extend its in vivo half-life, and slow or prevent its passive delivery to the target tissues, and is thus an essential factor for the in vivo performance of drugs in general [19, 23, 24]. In addition, albumin is known to accumulate in malignant and inflamed tissue through the so-called enhanced permeability and retention (EPR) effect due to a defective leaky vasculature combined with the absence of an effective drainage system, and interaction with HSA may eventually provide additional selectivity by passively targeting tumor tissues [24, 25]. This may be very important for future drug delivery. Nevertheless, understanding of the biological targets of metal complexes is of vital importance to tackle the severe side effects and the development of resistance by current chemotherapeutic drugs, as well as for the redesign of novel agents that target cellular signaling pathways specific to cancer cells.

Our group has previously shown that cobalt and zinc complexes bearing 1,10-phenanthroline-5,6-dione (phendione) in their coordination sphere exhibit very high antiproliferative activity against human colorectal (HCT116), hepatocellular (HepG2), and breast (MCF-7) tumor cell lines [26]. Indeed, the complexes $[Zn(phendione)_2]Cl_2$ and $[Co(Cl)(phendione)_2(H_2O)][BF_4]$ were approximately 70-fold and twofold more active against HCT116 tumor cells than the chemotherapeutic agents cisplatin and doxorubicin tested under the same conditions [26, 27]. This highlights the enhancing effect of the Co(II) ion on the performance of the latter (octahedral) complex and prompted us to explore further its potential as a viable metallodrug in the context of cancer therapy. The cobalt complex is used as the BF_4 salt to increase its stability, since tetrafluoroborate compounds are known to be relatively stable at room temperature [28]. Nevertheless, the water solubility of $[Co(Cl)(phendione)_2(H_2O)][BF_4]$ at 25 °C is 2.2 mg mL^{-1} [26].

The antiproliferative activity of the Co(II) complex was due to cell cycle arrest in S phase and subsequent cell death by apoptosis [27]. Furthermore, this complex displayed

P. M. Borralho · C. M. P. Rodrigues
Research Institute for Medicines and Pharmaceutical Sciences (iMed.UL), Faculdade de Farmácia, Universidade de Lisboa, Lisbon, Portugal

A. S. Rodrigues
Centro de Investigação em Genética Molecular e Humana, Departamento de Genética, Faculdade de Ciências Médicas, Universidade Nova de Lisboa, Lisbon, Portugal

A. R. Fernandes
Faculdade de Engenharia, Universidade Lusófona de Humanidades e Tecnologias, Lisbon, Portugal

lower activity in healthy human fibroblasts than in HCT116 cells, thus exhibiting higher cytotoxic activity in the malignant cell line [26]. Proteomic analysis of cancer cells exposed to this Co(II) complex showed upregulation of SODC, which correlated with higher levels of ROS in exposed HCT116 cells [27]. Exposure of HCT116 cells to this Co(II) complex also resulted in the downregulation of proteins usually upregulated in cancer cells, namely, HSPB1, GRP94, TCTP, C1QBP, LEG1, and PPIA [27]. Conversely, antiproliferative PA2G4 and apoptosis-related VDCA were found to be overexpressed in presence of the Co(II) complex [27]. These results demonstrate that this complex exhibits an excellent therapeutic potential by modulating the expression of proteins typically deregulated in tumors [27]. Nevertheless, information on the ability of this complex to interact with DNA or on the affinity towards albumin is of vital importance and was lacking. The latter aspect, in particular, is surely relevant for future targeted delivery to cancer cells. In this regard, the aim of the present study was to characterize further the mechanisms underlying the antiproliferative potential of $[Co(Cl)(phendione)_2(H_2O)][BF_4]$ by (1) evaluating the expression of antiapoptotic and proapoptotic players in the mechanism of cell death, (2) determining its affinity for DNA and the corresponding binding mode, (3) addressing its genotoxic potential in V79 cells and HCT116 cells, and (4) examining its interaction with HSA using steady-state and time-resolved fluorescence spectroscopy.

Materials and methods

Compound synthesis

The metal complex $[Co(Cl)(phendione)_2(H_2O)][BF_4]$ was synthesized and characterized as previously described [26]. All chemical reagents were used as received from the supplier without further purification. 4-(2-Hydroxyethyl)piperazine-1-ethanesulfonic acid (Hepes), NaH_2PO_4, Na_2HPO_4, and NaCl were purchased from Sigma-Aldrich (Spain). Millipore® water was used for the preparation of all aqueous solutions. Fatted HSA (from human plasma, A1653; 96–99 %, with a molecular mass of 66–67 kDa) and Ludox® were purchased from Sigma-Aldrich.

Cell culture

HCT116 human colorectal carcinoma cells were grown in Dulbecco's modified Eagle's medium (DMEM) (Invitrogen, Grand Island, NY, USA) supplemented with 10 % (v/v) fetal bovine serum and 1 % (v/v) antibiotic/antimycotic solution (Invitrogen) and maintained at 37 °C in a humidified atmosphere of 5 % CO_2. HepG2 human hepatocellular carcinoma cells were grown in similar conditions, supplemented with 1 % MEM nonessential amino acids (Invitrogen). V79 Chinese hamster pulmonary fibroblasts were grown in DMEM supplemented with 5 % (v/v) fetal bovine serum in 50-mL Falcon tubes tilted by 45° and maintained as described above. Nontumorigenic human mammary epithelial cells (MCF10A) were grown in DMEM/F12 (Gibco, Life Technologies, Spain) supplemented with 0.5 mg mL^{-1} hydrocortisone (Sigma), 5 % (v/v) horse serum (Invitrogen, Life Technologies, Spain), 20 ng mL^{-1} epidermal growth factor (Sigma), 100 ng mL^{-1} cholera toxin (Sigma), and 10 μg mL^{-1} insulin (Sigma).

Cell viability

MCF10A cells were plated at 5,000 cells per well in 96 well plates. Medium was removed 24 h after platting and was replaced with fresh medium containing 0.1–1 μM $[Co(Cl)(phendione)_2(H_2O)][BF_4]$ or water (vehicle control). After 48 h of cell incubation in the presence or absence of $[Co(Cl)(phendione)_2(H_2O)][BF_4]$, cell viability was evaluated with the CellTiter 96® AQueous nonradioactive cell proliferation assay (Promega, Madison, WI, USA), as previously described [29].

Caspase-3/7 activity

HCT116 cells were plated at 7,500 cells per well in a black opaque 96-well microplate (Corning). Medium was removed 24 h after platting and was replaced with fresh medium containing increasing concentrations of $[Co(Cl)(phendione)_2(H_2O)][BF_4]$ (0.20, 0.35, and 0.50 μM) or sterile water (vehicle control). The blank control was made with culture medium without cells. Cells were incubated for 48 h at 37 °C and 5 % CO_2. Combined caspase-3/7 activity was quantified using the Apo-ONE® homogeneous caspase-3/7 assay (Promega) according to the manufacturer's instructions. Briefly, 100 μL of the mixture containing the profluorescent substrate was added to each well and after incubation for 2 h at 37 °C and 5 % CO_2, fluorescence was measured in an Anthos Zenyth 3100 (Anthos Labtec Instruments) plate reader with excitation and emission wavelengths of 485 and 535 nm, respectively.

Lactase dehydrogenase activity

HepG2 cells were plated at 10,000 cells per well in 96-well plates. Culture medium was removed after 24 h and was replaced by fresh medium containing 1 μM $[Co(Cl)(phendione)_2(H_2O)][BF_4]$ or sterile water (vehicle control) and either with or without 100 μM ursodeoxycholic acid (UDCA). The bile acid was maintained as a

100 mM stock solution in dimethyl sulfoxide (DMSO). DMSO (0.1 %, v/v) was also used as a solvent control for UDCA. Cells were incubated for 48 h at 37 °C and 5 % CO_2. Lactase dehydrogenase (LDH) activity was assessed with the a Cytotoxicity Detection Kit^{PLUS} (LDH) (Roche), according to the manufacturer's instructions. One hundred microliters of supernatant from each sample was transferred to a new 96-well plate and mixed with 100 µL of reaction mixture containing the colorimetric substrate of LDH, and was allowed to react for 10 min at room temperature. The absorbance of the colored reaction product was measured at 490 nm in a model 680 microplate reader (Bio-Rad).

Real-time PCR

Cells were seeded into 25-cm^2 culture flasks at 1×10^5 cells per flask. After 24 h of incubation at 37 °C and 5 % CO_2 the culture medium was replaced by fresh medium containing either 0.35 µM [Co(Cl)(phendione)$_2$(H_2O)][BF_4] or sterile water (vehicle control). Cells were incubated for 48 h at 37 °C and 5 % CO_2, pelleted, and washed with 1× phosphate-buffered saline (PBS). Total RNA was extracted directly from the cell pellet using an SV total RNA isolation system (Promega) and converted into complementary DNA (cDNA) using a cDNA synthesis kit (Bioline), both according to the manufacturers' instructions. The concentration and purity of RNA and cDNA were analyzed with a NanoDrop 2000 spectrophotometer (Thermo Scientific, Waltham, MA, USA). One microgram of single-stranded cDNA was used as a template for the amplification of genes involved in cell cycle and apoptosis regulation by using a SensiFast SYBR No-ROX kit (Bioline) according to the manufacturer's instructions. Real-time reverse transcription PCRs were conducted in a LightCycler 480 (Roche) using the following conditions: enzyme activation at 95 °C for 2 min (single step), and denaturation at 95 °C for 5 s, annealing at 59–65 °C for 10 s and extension at 72 °C for 10 s, for a total of 35 cycles. Primer sequences and specific annealing temperatures can be found in Table 1. Variations in gene expression were calculated by applying the $\Delta\Delta C_t$ method [30]. To confirm the absence of unspecific amplification, PCR products (2 µL per sample) were analyzed by electrophoresis in 2 % (w/v) agarose gel stained with RedGel (Biotium) for 50 min at 110 V.

DNA UV titrations

The interaction mechanism and binding affinity of [Co(Cl)(phendione)$_2$(H_2O)][BF_4] with calf thymus DNA (CT-DNA) (Invitrogen) was studied by UV spectroscopy as previously described [29]. The dilution effect as a result of the addition of the DNA solution was corrected and the affinity constants were calculated according to Eq. 1:

$$\frac{[\mathrm{DNA}]}{\varepsilon_a - \varepsilon_f} = \frac{[\mathrm{DNA}]}{\varepsilon_b - \varepsilon_f} + \frac{1}{K_b(\varepsilon_b - \varepsilon_f)}, \quad (1)$$

where [DNA] is the concentration of CT-DNA (per nucleotide phosphate), $\varepsilon_a = \mathrm{Abs}/[\mathrm{complex}]$, ε_f is the extinction coefficient for the free complex, and ε_b is the extinction coefficient for [Co(Cl)(phendione)$_2$(H_2O)][BF_4] when fully bound to DNA. DNA concentration (expressed as the molarity of phosphate groups) was determined with a NanoDrop 2000 spectrophotometer assuming $\varepsilon_{260} = 6{,}600\ \mathrm{M}^{-1}\ \mathrm{cm}^{-1}$ [33].

Electrophoretic analysis of DNA–metal complex interaction

Plasmids were obtained from *Escherichia coli* transformed cells, grown overnight in a Luria–Bertani liquid medium (AppliChem, Darmstadt, Germany) with 100 µg mL^{-1} ampicillin (Bioline, London, UK), at 37 °C with stirring. Plasmid extractions were performed using an Invisorb® Spin Plasmid Mini Two kit (Invitek, Berlin, Germany) and DNA was quantified by spectrophotometry with a NanoDrop 2000 spectrophotometer. The interactions between [Co(Cl)(phendione)$_2$(H_2O)][BF_4] and pBluescript II SK(+) (pBSK II) DNA (Agilent Technologies, Santa Clara, CA,

Table 1 Primers and annealing temperatures used for real-time reverse-transcription PCRs

Gene	Encoded protein	Forward primer (5′–3′)	Reverse primer (5′–3′)	T_{Ann} (°C)	Product size (bp)	Reference
CDKN1A	p21	GCTTCATGCCAGCTACTTCC	AGGTGAGGGGACTCCAAAGT	59	221	Present work
RNA18S5	Ribosomal major subunit	GTAACCCGTTGAACCCCATT	CCATCCAATCGGTAGTAGCG	59	151	
BAX	Bax	TGCTTCAGGGTTTCATCCAGGA	ACGGCGGCAATCATCCTCTG	62	172	[31]
BCL2	Bcl-2	CTTCGCCGAGATGTCCAGCCA	CGCTCTCCACACACATGACCC	65	152	
CASP3	Caspase-3	TACCAGTGGAGGCCGACTTC	GCACAAAGCGACTGGATGAAC	59	103	
CCNE2	Cyclin E2	GAATGTCAAGACGAAGTA	ATGAACATATCTGCTCTC	60	380	[32]

USA) and pUC18 (2,686 bp) (Fermentas, USA) were determined as previously described [29].

For the concentration dependence studies, pBSK II (200 ng in a final volume of 20 μL) was incubated in the presence (25–100 μM) or absence of the test compound for 24 h at 37 °C in reaction buffer [5 mM tris(hydroxymethyl)aminomethane (Tris)–HCl, 50 mM NaCl pH 7.02]. For the time course studies, pBSK II (400 ng) was incubated with 250 μM $[Co(Cl)(phendione)_2(H_2O)][BF_4]$ and in its absence at 37 °C in reaction buffer, for a final volume of 20 μL per reaction. Reactions were stopped by adding loading buffer [25 mM Tris–HCl, 25 mM EDTA (pH 8.0), 50 % glycerol, 0.1 % bromophenol blue] and the reaction mixtures were chilled immediately in an ice–ethanol bath at zero time and after 5, 10, 15, 20, and 30 min of incubation. Untreated plasmid DNA (pDNA) was incubated for 30 min. For the evaluation of base-specific interaction with DNA, 30 μM (per nucleotide phosphate), plasmid pUC18 (Fermentas) treated with the test compound at 3 μM ($r = 0.1$) and 9 μM ($r = 0.3$) in a final volume of 20 μL was digested with the restriction enzymes *Dra*I and *Sma*I as previously described [29].

Compound–DNA interaction assays were performed in tubes containing 200 ng of pDNA and $[Co(Cl)(phendione)_2(H_2O)][BF_4]$ at different concentrations in the presence and in the absence of the activating agent H_2O_2 (200 μM). Then 5 mM Tris–HCl buffer (Merck), 50 mM NaCl (Panreac), pH 7.0, was added to a final volume of 20 μL. A control sample was also prepared with pDNA and buffer using the same method as described above. A typical reaction mixture, containing supercoiled pDNA and $[Co(Cl)(phendione)_2(H_2O)][BF_4]$ in 5 mM Tris–HCl (Merck), 50 mM NaCl (Panreac), pH 7.0, was incubated at 37 °C for 4 or 24 h (with or without additives, or without any external reductant). After the incubation, reactions were quenched by keeping the samples at −20 °C followed by addition of 4 μL of loading buffer [25 mM Tris–HCl, 25 mM EDTA (pH 8.0), 50 % glycerol, 0.1 % bromophenol blue]. Samples were then loaded on a 0.8 % agarose gel (p/v) (SeaKem® LE agarose, Lonza, Rockland, ME, USA) dissolved in 1× 4.84 g Tris base (Merck), 0.5 M EDTA (Riedel-de Haën), 1.142 mL acetic acid (Panreac), pH 8.0 (TAE buffer). Electrophoresis was performed at 80 V as a constant voltage for 2 h in 1× TAE buffer. DNA was stained by immersing the agarose gel in an ethidium bromide solution (0.5 mg L^{-1} in distilled water) for 20 min. Afterwards the gel was washed in distilled water for 10 min and the results were analyzed and photographed using a UVITEC (Cambridge, UK) transilluminator coupled to a Kodak Alpha-DigiDoc camera (Alpha Innotech, Santa Clara, CA, USA). For the concentration and time dependence studies of DNA cleavage, the different forms of the plasmid were quantified by densitometry analysis using GelAnalyzer 2010a.

T4 DNA ligation studies

Plasmid pcDNA3-*eGFP* (plasmid 13031, Addgene, Cambridge, MA, USA) was amplified in the *E. coli* DH5α host culture grown overnight in Luria–Bertani broth (AppliChem, Darmstadt, Germany) supplemented with 100 μg mL^{-1} ampicillin (Bioline, London, UK) at 37 °C with orbital shaking. The plasmid was purified using an NZYMiniprep kit (NZYTech, Lisbon, Portugal) according to the manufacturer's instructions. Plasmid DNA (pDNA) religation experiments were performed using T4 DNA ligase to support the hydrolytic mechanism of DNA cleavage by following the standard DNA religation protocol. First, 200 ng of pcDNA3-*eGFP* was incubated in the presence or absence of $[Co(Cl)(phendione)_2(H_2O)][BF_4]$ (100 μM) in the reaction buffer (5 mM Tris–HCl, 50 mM NaCl pH 7.02) (final volume of 20 μL) for 24 h at 37 °C. Then, 100 ng of the resulting product was ligated by T4 DNA ligase by adding 2 μL of 10× reaction buffer (660 mM Tris–HCl, pH 7.6, 66 mM $MgCl_2$, 100 mM dithiothreitol, 660 mM ATP) (NZYTech), 1 μL of T4 DNA ligase (5 U μL^{-1}) (NZYTech), and nuclease-free water to a final volume of 20 μL.

The reaction was performed 1 h at room temperature. Electrophoresis was performed in a 0.7 % agarose gel (w/v) dissolved in 1× TAE buffer and stained with RedGel at 80 V for 2 h. Gels were illuminated from below with UV light and photographed using the GelDoc and the Quantity One computer programs (Bio-Rad). DNA-bound ethidium bromide in the gel unwinds and therefore resolves relaxed closed, religated DNA from the nicked circular form. DNA mobility for each form was determined by comparison with religated controls (DNA nicked initially by *Eco*RI and then religated).

Chromosomal aberrations

V79 cells (1×10^6) were treated with 1.5 μM mitomycin C and 0.25, 0.5, and 1 μM $[Co(Cl)(phendione)_2(H_2O)][BF_4]$ for 16 h at 37 °C and 5 % CO_2. After 14 h incubation, 0.1 mL of a 4 mg mL^{-1} colchicine solution was added to each sample. Cell suspensions were then homogenized and incubated for another 2 h. Cells were harvested by centrifugation (1,500 rpm for 5 min), and 8 mL of a prewarmed (37 °C) 75 μM KCl solution was added to each pellet. Samples were thawed in a water bath at 37 °C for 4 min, centrifuged (1,500 rpm for 5 min), and incubated for 15 min at −20 °C with 5 mL of a prechilled (−20 °C) solution of 3:1 (v/v) methanol/acetic acid (fixing solution). Cells were washed twice with the fixing solution and were resuspended in 3 mL of this same solution. Each cell suspension was mounted on a glass slide, and chromosomal aberrations were evaluated under a bright-field microscope by using Giemsa staining.

Genotoxicity assessment

Genotoxic effects were assessed by quantification of DNA strand breakage through the alkaline version of the comet assay and the frequency of nuclear abnormalities [34]. HCT116 cells were plated at 10^6 cells per dish in 35-mm dishes and were allowed to attach for 24 h at 37 °C and 5 % (v/v) CO_2. Culture medium was removed and replaced with 2 mL of fresh medium containing either 0.20 μM $[Co(Cl)(phendione)_2(H_2O)][BF_4]$ or 0.1 % (v/v) H_2O (negative control) for 12 and 18 h at 37 °C and 5 % (v/v) CO_2. Hydrogen peroxide was used as a positive control at 0.05 % (v/v) for 30 min at room temperature. Glass microscope slides were initially prepared with a coating of 1 % (w/v) agarose (normal melting point agarose) in 1 ×TAE buffer and left to solidify at 37 °C for at least 48 h. Cells were harvested by scrapping, and cell density was determined by the trypan blue dye exclusion assay. Solutions of 1×10^5 cells per milliliter in 1× PBS were prepared, and from these 10 μL was added to 90 μL of 1 % (w/v) low melting point agarose in 1× PBS and dropped on the slides prepared previously, resulting in a density of 10^4 cells per slide. A coverslip was used to spread the sample across the agarose layer, and the slides were allowed to dry at 4 °C for 15 min. On solidification of agarose, the coverslips were removed and the slides were dipped into lysis solution [450 mM NaCl, 3.72 % EDTA, 5 mM Tris; to which 10 % (v/v) DMSO and 1 % (v/v) Triton-X were added just before use] for 1 h at 4 °C, followed by their being dipped for 40 min into cold electrophoresis solution (1 mM EDTA, 300 mM NaOH, pH 13) to ensure DNA unwinding and promote expression of alkali-labile sites. Electrophoresis was performed at 4 °C for 30 min at 25 V using a Sub-Cell model 96 apparatus (Bio-Rad). Afterwards, slides were placed in 0.1 M Tris–HCl buffer (pH 7.5) at 4 °C for 15 min for neutralization, followed by 15 min in methanol at 4 °C and drying at 37 °C. For visualization of comets, slides were hydrated with distilled water at 4 °C for 30 min and stained with 20 μL of an ethidium bromide working solution (20 μg mL^{-1}) and covered with new coverslips. The slides were observed under a Leica DFC 480 fluorescence microscope (Leica Microsystems, Cambridge, UK) and analyzed by CometScore version 1.5 (TriTek). About 100 cells per sample were analyzed. The percentage of DNA in the tail was used as a measure of the total DNA strand breakage.

Sample preparation for spectroscopic measurements with albumin

HSA stock solutions were prepared by gently dissolving the protein in phosphate buffer pH 7.0 with 0.15 M NaCl. A time of 45–60 min was needed to allow the protein to hydrate and fully dissolve (in the concentration required for stock solutions, less than 100 μM), the solution being gently swirled from time to time. The concentration of each HSA stock solution was determined by UV spectrophotometry using a molar extinction coefficient of $\varepsilon_{278\text{-}nm} = 36{,}850\ M^{-1}\ cm^{-1}$ [35].

Spectroscopic measurements were conducted on individually prepared samples to ensure the preincubation time at (37.0 ± 0.5) °C was the same in each essay. Samples were prepared from a $[Co(Cl)(phendione)_2(H_2O)][BF_4]$ stock solution in buffer by appropriate dilution. For UV–vis spectroscopy, the HSA concentration was 15.0 μM and the molar ratio of HSA to $[Co(Cl)(phendione)_2(H_2O)][BF_4]$ used was 1:1 and 1:2. For fluorescence measurements, the HSA concentration was kept constant at 2.0 μM, whereas the concentration of $[Co(Cl)(phendione)_2(H_2O)][BF_4]$ ranged from 0 to 30.03 μM. Samples were incubated at 37 °C for 24 h. To ensure the incubation time and the measurement conditions were the same (e.g., same exposure to excitation radiation), the solutions containing protein and each Co(II) concentration were prepared separately from the stock solutions.

Spectroscopic measurements

UV–vis absorption spectra were recorded at room temperature with a V-560 spectrophotometer (JASCO, Hiroshima, Japan) in the range from 230 to 500 nm with 1 cm path length quartz Suprasil® cuvettes.

Fluorescence measurements were performed with a Spex FL-1057 Tau 3 spectrofluorometer from Horiba Jobin Yvon at room temperature. Details on sample preparation are given in the previous subsection. Samples with the same concentration of the complex but with no protein were prepared for appropriate background correction. For steady-state fluorescence intensity measurements, excitation was at 295 nm. The fluorescence intensity was corrected for the absorption and emission inner filter effect using the UV–vis absorption data recorded for each sample [36]. The bandwidth was typically 5 nm in both excitation and emission. For time-resolved measurements by the single photon counting technique, a nanoLED N-280 (Horiba Jobin Yvon) was used for the excitation of HSA and the emission wavelength was 340 nm with a 15-nm bandwidth using a detection system with 50-ps resolution. Ludox® was used as the scatterer to obtain the instrumental response function. The program TRFA Data Processor version 1.4 (Scientific Software Technologies Center, Minsk, Belarus) was used for the analysis of the experimental fluorescence decays. The fluorescence intensity decays were analyzed by fitting a sum of exponentials according to Eq. 2:

$$I(t) = \sum_{i=1}^{n} \alpha_i \exp(-t/\tau^i), \quad (2)$$

where α_i and τ_i are the normalized amplitude and lifetime of component i, respectively.

The changes in quantum yield caused by processes affecting the fluorescence lifetime were evaluated from the amplitude-weighted mean fluorescence lifetime, which is given by Eq. 3:

$$\bar{\tau} = \sum_{i=1}^{n} \alpha_i \tau_i \quad (3)$$

The quality of the fit was evaluated by a reduced χ^2 value close to 1 and random distribution of weighted residuals and residual autocorrelation.

Results and discussion

In our previous study, the [Co(Cl)(phendione)$_2$(H$_2$O)][BF$_4$] (Fig. 1) was shown to have lower cytotoxicity in healthy human fibroblasts than in HCT116 tumor cells [26]. Since fibroblasts are connective-tissue cells, we also tested cell viability in MCF10A, a nontumorigenic epithelial cell line from mammary gland (Fig. S1). The half-maximal inhibitory concentration (IC_{50}) obtained for this cell line, (5.14 ± 0.01) μM, is more than 6.9 times higher than that determined for the tumorigenic breast cell line MCF7 (0.73 μM) [26]. This value is even higher (25 and 8.6 times, respectively) when compared with the IC_{50} values for HCT116 (0.21 μM) and HepG2 (0.58 μM) [26]. Since all the previously tested tumor cell lines were of the epithelial type [26], this result may indicate increased cytotoxic activity in tumor cells compared with healthy cells.

To confirm the role of [Co(Cl)(phendione)$_2$(H$_2$O)][BF$_4$] in the induction of apoptosis as previously observed by our group [27], combined caspase-3/7 activity was determined in HCT116 cells exposed to [Co(Cl)(phendione)$_2$(H$_2$O)][BF$_4$]. For all concentrations tested, caspase-3/7 activity increased by more than 50 % compared with the control. However, at 0.5 μM, there was a slight decrease in caspase activity, possibly indicating a significant drop in the viable cell population that partially offset the expected increase in caspase-3/7 activity. Flow cytometry data showed that cells treated with 0.2 and 0.35 μM [Co(Cl)(phendione)$_2$(H$_2$O)][BF$_4$] exhibited an extremely low level of necrosis [27], whereas those incubated with 1 μM [Co(Cl)(phendione)$_2$(H$_2$O)][BF$_4$] exhibited a higher amount of viability loss and 3.2 times more necrotic cells than in the vehicle control [27] (results not shown). From these findings, the slight reduction of caspase-3/7 activity observed at 0.5 μM (compared with 0.2 and 0.35 μM) may result from the combined effect of a lower number of viable cells (smaller amount of total protein) and an increase in cell death by necrosis [27] (results not shown). Nevertheless, at this concentration (0.5 μM), the level of caspase-3/7 activity is still higher than that of control cells (Fig. 2). Reduction of caspase activity for levels of cell stress has already been seen for other types of compounds, such as hydrogen peroxide [37]. It was shown that at 50 μM hydrogen peroxide there was an increase of caspase activity, but at higher concentrations of hydrogen peroxide there was no detectable caspase activity, and the cells died by necrosis [37].

UDCA is a hydrophilic bile acid with demonstrated antiapoptotic activity in both in vitro and in vivo models [38]. To understand if UDCA is able to reverse the cytotoxicity of [Co(Cl)(phendione)$_2$(H$_2$O)][BF$_4$], LDH release into the culture medium in HepG2 cells incubated in the presence or absence of UDCA and [Co(Cl)(phendione)$_2$(H$_2$O)][BF$_4$] was measured (Fig. 3). LDH is commonly used to determine cell viability/death, since LDH does not leak out from healthy cells; hence, LDH activity in culture medium derives from leakage from dead cells

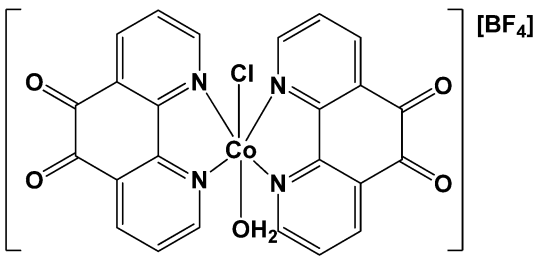

Fig. 1 Structure of [Co(Cl)(H$_2$O)(phendione)$_2$][BF$_4$] (phendione is 1,10-phenanthroline-5,6-dione)

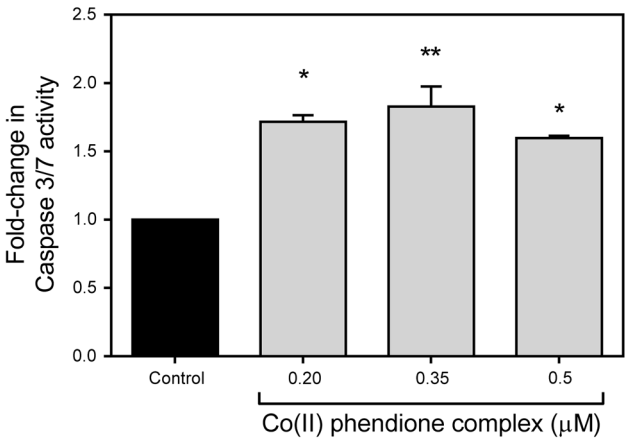

Fig. 2 Increased activity of effector caspases-3/7-like activity in HCT116 cells following exposure to [Co(Cl)(phendione)$_2$(H$_2$O)][BF$_4$] for 48 h. *Asterisks* indicate significant differences between the control sample and samples treated with [Co(Cl)(phendione)$_2$(H$_2$O)][BF$_4$]: *one asterisk* $p < 0.001$; *two asterisks* $p < 0.005$

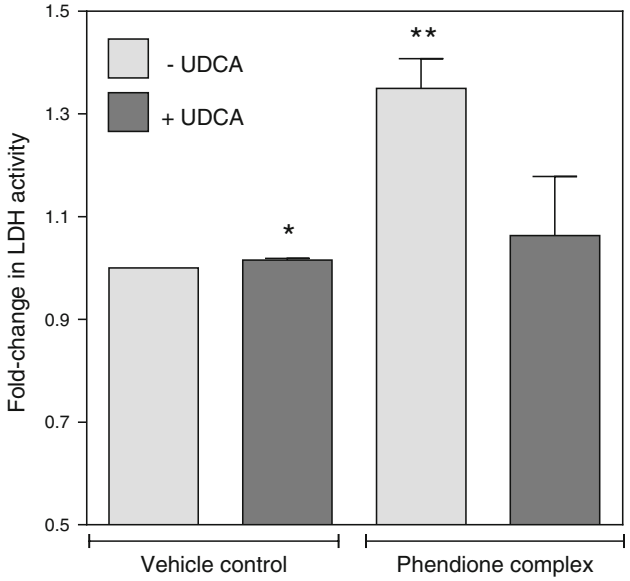

Fig. 3 Comparison of lactate dehydrogenase (*LDH*) activity in HepG2 cells treated with 1 μM $[Co(Cl)(phendione)_2(H_2O)][BF_4]$ with or without 100 μM ursodeoxycholic acid (*UDCA*) for 48 h. *Asterisks* indicate significant differences in LDH activity between control (sterile water; − *UDCA*) and treated samples: *one asterisk* $p < 0.05$; *two asterisks* $p < 0.005$

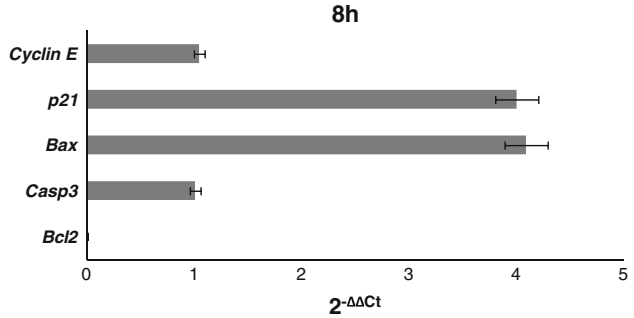

Fig. 4 Fold change in expression levels of cyclin E, p21, Bax, caspase-3 (*Casp3*) and Blc-2 in HCT116 tumor cells exposed to 0.35 μM $[Co(Cl)(phendione)_2(H_2O)][BF_4]$ for 8 h relative to untreated samples. The expression level of 18S ribosomal RNA was used as an internal control to correct for variations in the total RNA amount between samples. The values are the mean of at least two independent experiments. *Error bars* indicate the standard error of the mean (SEM)

only [39]. As observed in Fig. 3, most of the induction of LDH release by $[Co(Cl)(phendione)_2(H_2O)][BF_4]$ in HepG2 cells was reduced when cells were co-incubated with UDCA, indicating a lesser extent of cell death in this condition. Interestingly, reversible apoptotic events were previously well characterized by other authors [40, 41]. Tang et al. [40] showed that apoptotic dying cancer cells regained normal morphology and proliferate after the removal of the apoptosis inducer. This reversibility of cancer cells from apoptosis raised the question whether apoptotic recovery contributes to the survival or repopulation of cancer after cycles of chemotherapy [40].

UDCA is a bile acid with known cytoprotective properties [42]. Both inhibition of apoptosis and activation of survival pathways have been proposed for the protective effect of UDCA [42]. UDCA negatively modulates the mitochondrial pathway by inhibiting Bax translocation, ROS formation, cytochrome *c* release, and caspase-3 activation. In addition, UDCA may also interfere with the death receptor pathway, inhibiting caspase-3 activation. Importantly, UDCA interacts with nuclear steroid receptors (NSR), leading to NSR/hsp90 dissociation and nuclear translocation of the UDCA–NSR complex. In the nucleus, UDCA modulates the E2F-1/p53/Bax pathway, thereby preventing apoptosis. Finally, UDCA also downregulates cyclin D1 and Apaf-1, further inhibiting the mitochondrial apoptotic cascade [42]. The protein p53 was established as a key molecular target in UDCA prevention of cell death [43]. The pretreatment of primary rat hepatocytes with UDCA abrogated all apoptotic changes induced by p53 overexpression, such as Bax mitochondrial translocation, cytochrome *c* release, and caspase-3 activation. More importantly, an increased association between p53 and Mdm2 was also detected. By inducing Mdm2–p53 complex formation, UDCA reduces p53 activity, simultaneously blocking its transactivation domain and enhancing its export to the cytosol. The pivotal role of Mdm2 in the antiapoptotic properties of UDCA was confirmed by Mdm2 silencing. Nevertheless, the precise mechanism by which UDCA induces Mdm2–p53 binding remains to be determined [42].

Regression of tumor mass by chemotherapy is caused by growth suppression and/or apoptosis of tumor cells [44]. Therefore, expression levels of cell cycle and apoptosis molecules (cyclin D1 and cyclin E and caspase-3, Bax, and p21) should be predictive markers for the efficacy of a drug [44]. In the present study, the expression levels of key molecules involved in cell cycle regulation and apoptosis were evaluated in the HCT116 tumor cell line exposed to 0.35 μM $[Co(Cl)(phendione)_2(H_2O)][BF_4]$ (or no-addition control) for 8 h (Fig. 4). As we can observe in Fig. 4, HCT116 cells strongly express p21 and Bax, demonstrating sensitivity to $[Co(Cl)(phendione)_2(H_2O)][BF_4]$.

Despite the increased expression of p21 and Bax, caspase-3 and cyclin E expression did not show any variation after 8 h of exposure to $[Co(Cl)(phendione)_2(H_2O)][BF_4]$ (Fig. 4). Nevertheless, in order to understand if this expression was time-dependent, the caspase-3 expression level was also assessed after 4 h exposure to 0.35 μM $[Co(Cl)(phendione)_2(H_2O)][BF_4]$, and was found to show a slight increase ($2^{-\Delta\Delta C_t} = 1.5 \pm 0.03$) (data not shown). In addition, the assessment of p21 and Bax expression in the

HCT116 tumor cell line may represent a useful factor as this expression indicates a response of the cells to [Co(Cl)(phendione)$_2$(H$_2$O)][BF$_4$]. The protein p21 plays an essential role in growth arrest after DNA damage, and its overexpression leads to G_1- and G_2-phase arrest or S-phase arrest [45]. Indeed, our previous results showed an S-phase arrest following exposure to this metal complex [27] that can progress to cell death by apoptosis, as caspase-3 activity and p21-mediated cleavage increase. Furthermore, the downregulation of Bcl-2, an antiapoptotic protein, in the presence of [Co(Cl)(phendione)$_2$(H$_2$O)][BF$_4$]is also in agreement with the reported induction of apoptosis (Fig. 4).

Our data clearly demonstrate that exposure to [Co(Cl)(phendione)$_2$(H$_2$O)][BF$_4$] markedly increases the expression of the genes encoding p21 and Bax, both of which are p53-inducible genes. Therefore, it is possible that [Co(Cl)(phendione)$_2$(H$_2$O)][BF$_4$] may increase expression and/or activation of p53, which would account for the increased expression of p21 and Bax, and for apoptosis induction. In contrast, the ability of UDCA to reduce of the cytotoxicity of [Co(Cl)(phendione)$_2$(H$_2$O)][BF$_4$] may result from a stabilization of the interaction of p53 with Mdm2, which may lead to a reduced p53 transcriptional activity and consequent reduced p21 and Bax expression, and cell death. However, UDCA may also be exerting its cytoprotective effect by mechanisms other than those described above; it would be interesting to explore the detailed mechanism of cytoprotection by UDCA following exposure of cells to t[Co(Cl)(phendione)$_2$(H$_2$O)][BF$_4$] in future studies.

To understand if [Co(Cl)(phendione)$_2$(H$_2$O)][BF$_4$] is able to interact with DNA, titration of [Co(Cl)(phendione)$_2$(H$_2$O)][BF$_4$] with CT-DNA was monitored by UV spectroscopy (Fig. 5). As shown in Fig. 5, a hypochromic effect was observed, i.e., a decrease of the absorbance with the increase of DNA concentration in solution. Additionally, no or negligible hypsochromic or bathochromic shifts were observed on addition of DNA to the [Co(Cl)(phendione)$_2$(H$_2$O)][BF$_4$] solution. According to Ramakrishnan et al. [46], a bathochromic shift associated with hypochromism results from the stacking of ligands with DNA bases during intercalation, whereas the hypochromism alone is related to the binding of a small molecule to DNA grooves through hydrophobic interactions. This would imply a groove binding mechanism for [Co(Cl)(phendione)$_2$(H$_2$O)][BF$_4$], on the basis of the absorbance variation obtained (Fig. 5). The intercalating agent doxorubicin produced, however, an equivalent profile, with hypochromism and no bathochromic shift (Fig. S2). The spectroscopic data are hence suggestive of either an intercalating or a groove binding mode for the interaction of [Co(Cl)(phendione)$_2$(H$_2$O)][BF$_4$] with DNA. In addition, the interaction studies with pDNA showed no reduction in the migration of the supercoiled form with increasing concentrations of the complex (Fig. 6a). The stacking of an intercalating agent with the DNA bases would result in an unwinding of the DNA double helix, consequently reducing its degree of supercoil and electrophoretic migration. Hence, a groove binding mechanism may be suggested for [Co(Cl)(phendione)$_2$(H$_2$O)][BF$_4$]. The affinity constant was determined on the basis of the above-mentioned absorbance decrease, obtained as a result of DNA–complex interaction. The calculated value for [Co(Cl)(phendione)$_2$(H$_2$O)][BF$_4$] [$K_b \pm$ the standard error of the mean (SEM) $(2.05 \pm 0.03) \times 10^5$ M^{-1}] (Fig. 5) is of the same magnitude as although roughly half of that determined for doxorubicin, a commonly used chemotherapeutic agent, under the same conditions [$K_b \pm$ SEM $(3.48 \pm 0.03) \times 10^5$ M^{-1}] (Fig. S2).

The higher level of p21 expression indicates that DNA damage may occur in the presence of [Co(Cl)(phendione)$_2$(H$_2$O)][BF$_4$]. In this regard, incubation of the pBSK II pDNA with increasing concentrations of [Co(Cl)(phendione)$_2$(H$_2$O)][BF$_4$] (25–100 μM) was performed (Fig. 6). A decrease of the supercoiled fraction of the pDNA with a proportional increase of the linear form and no significant variation of the relaxed circular form was observed (Fig. 6). Hence, these results might indicate that [Co(Cl)(phendione)$_2$(H$_2$O)][BF$_4$] acts as a double-strand cleaving agent, inducing double-strand breaks in DNA that result in a direct conversion of the supercoiled form of the plasmid into the linear one. Additionally, the time course studies revealed that a fraction of the supercoiled form of pBSK II was readily linearized by [Co(Cl)(phendione)$_2$(H$_2$O)][BF$_4$], and then linearization proceeds more slowly over time (Fig. 7). The time course data also demonstrate that the linearization of the plasmid does not result from the accumulation of single-strand breaks since that would require an increase in the amount of the circular relaxed form prior to that of the linear form, and our data show that there is no accumulation of the former even for $t \approx 30$ min (Fig. 7).

The disappearance of the supercoiled form, on its conversion into the linear form, follows pseudo-first order kinetics (Fig. 7c) with an apparent first-order rate constant (k_{obs}) of 6.06×10^{-3} min^{-1} for supercoiled DNA cleavage, given by the slope of the linear regression. The half-life ($t_{1/2}$) of the supercoiled form, i.e., the time at which 50 % of the pDNA is still in form I, was derived from the calculated k_{obs} and was determined to be approximately 114 min.

To further characterize the DNA binding mode of [Co(Cl)(phendione)$_2$(H$_2$O)][BF$_4$], the selective binding to the DNA bases guanine and cytosine or thymine and adenine was evaluated regarding the possible loss of specific

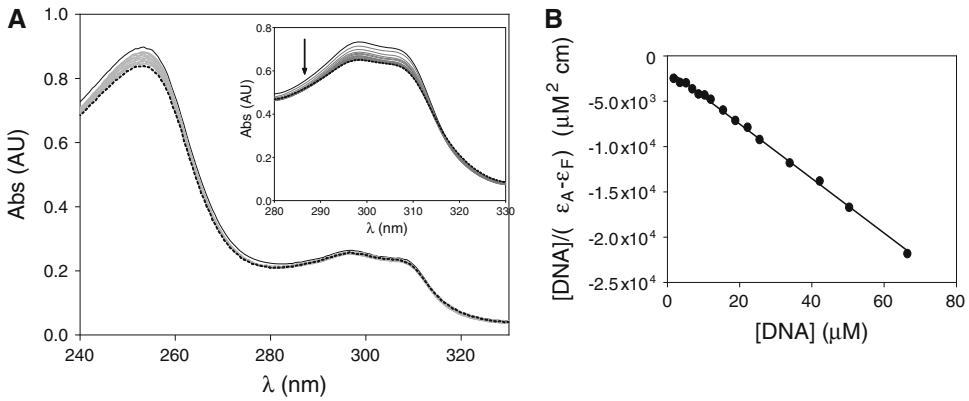

Fig. 5 UV titration of [Co(Cl)(phendione)$_2$(H_2O)][BF_4] with calf thymus DNA (CT-DNA). **a** UV spectra of the complex in the absence (*solid black line*) and presence of increasing amounts of CT-DNA. The spectrum that results from the highest DNA concentration is presented as a *dashed line*. The *inset* shows the UV spectrum used for the quantification of the binding strength. **b** Application of Eq. 1 to the determination of the DNA affinity constant, based on spectral variation at 298 nm (*inset* spectrum in **a**) on addition of CT-DNA

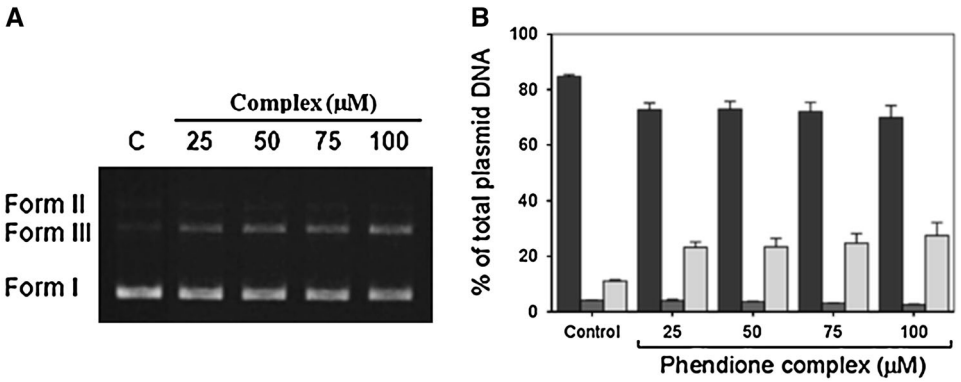

Fig. 6 Electrophoretic evaluation of DNA double-strand cleavage by [Co(Cl)(phendione)$_2$(H_2O)][BF_4]: conversion of supercoiled pBluescript II SK(+) (pBSK II) directly in its linear form by incubation with increasing concentrations of the test compound. **a** Electrophoretic distribution of the three plasmid forms in an agarose gel (0.7 %; w/v) as a result of exposure to 25–100 μM complex. All reactions were conducted in 5 mM tris(hydroxymethyl)aminomethane (Tris)–HCl, 50 mM NaCl, pH 7.02 for 24 h at 37 °C. For pBSK II plasmid DNA (pDNA), *C* refers to untreated pDNA, *form I* refers to the supercoiled form of pDNA, *form II* refers to the relaxed circular form of pDNA, and *form III* refers to the linear form of pDNA. **b** Densitometric quantification of plasmid forms using the image analysis program GelAnalyzer 2010a. *Black bars* represent the supercoiled form of pDNA and *gray bars* represent the linear form of pDNA. The results are expressed as the mean ± SEM of three independent experiments

restriction sites that may arise from base-specific binding of [Co(Cl)(phendione)$_2$(H_2O)][BF_4] [47]. Determination of base specificity was performed through the identification of fragments that result from enzymatic digestion of DNA with two restriction enzymes, *Sma*I and *Dra*I, that recognize GC-rich and TA-rich sequences, respectively [47]. The plasmid pUC18 has one recognition site for *Sma*I and three recognition sites for *Dra*I, respectively, producing one fragment (2,686 bp) and three fragments (1,975, 692, and 19 bp) after enzymatic digestion of DNA with these enzymes. The digestion pattern obtained (Fig. S3) showed no variation between pUC18 samples treated with [Co(Cl)(phendione)$_2$(H_2O)][BF_4] and untreated pUC18 samples, with one fragment in all samples digested with *Sma*I and two fragments in all samples digested with *Dra*I, since the 19-bp fragment was not observed in the 0.8 % (w/v) agarose gel.

To obtain insight into the nature of the pDNA cleavage observed in the presence of [Co(Cl)(phendione)$_2$(H_2O)][BF_4] (Fig. 6), we studied the effect of an oxidant, H_2O_2, and reductants (Fig. 8). The incubation of pDNA with [Co(Cl)(phendione)$_2$(H_2O)][BF_4] in the presence of H_2O_2, a known hydroxyl radical source, for 4 or 24 h seems to increase the amount of the linear form (form III), reducing the amount of the supercoiled form (form I) (Fig. 8, lanes 2 and 3 vs lanes 5 and 4, respectively), suggesting that [Co(Cl)(phendione)$_2$(H_2O)][BF_4] cleaves DNA more efficiently in the presence of an oxidant and the involvement of free radicals. The production of a hydroxyl radical owing to the reaction between

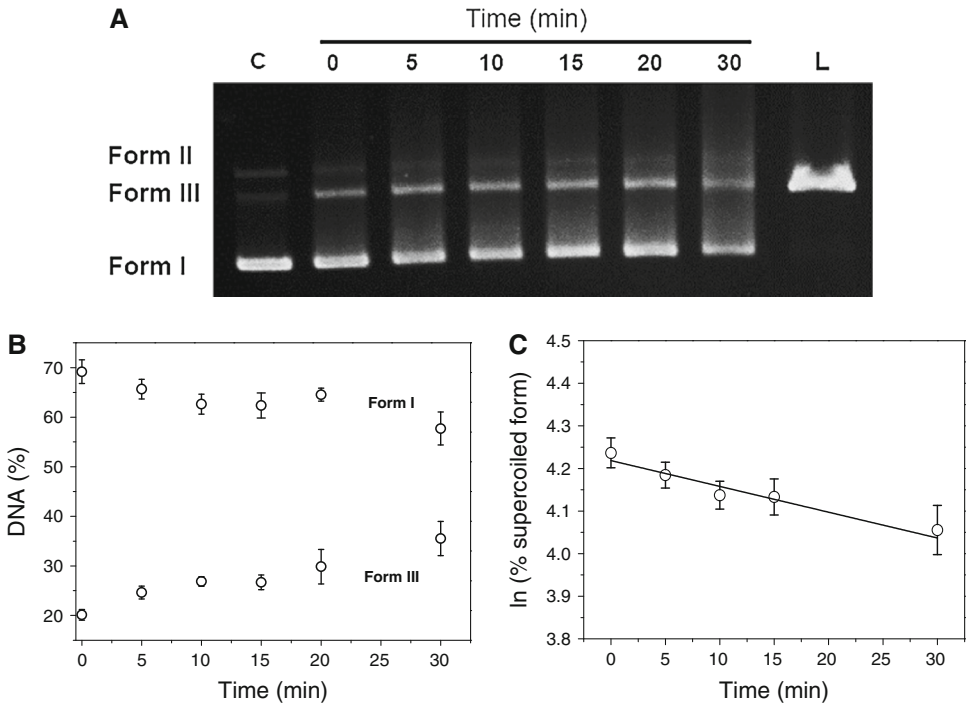

Fig. 7 Time course of pBSK II pDNA double-strand cleavage by [Co(Cl)(phendione)$_2$(H$_2$O)][BF$_4$] at pH 7.0 and 37 °C in 5 mM Tris–HCl, 50 mM NaCl. **a** Agarose gel [0.7 % (w/v)] of pBSK II (400 ng) incubated with [Co(Cl)(phendione)$_2$(H$_2$O)][BF$_4$] (250 μM) for the indicated periods of time. *Lane C* pDNA incubated for 30 min in the absence of [Co(Cl)(phendione)$_2$(H$_2$O)][BF$_4$], *lane L* linearized pDNA with *Eco*RI. **b** Densitometric quantification of pBSK II DNA forms by GelAnalyzer 2010a. **c** Plasmid cleavage kinetics: linear simulation of a pseudo-first-order reaction for the disappearance of the supercoiled form

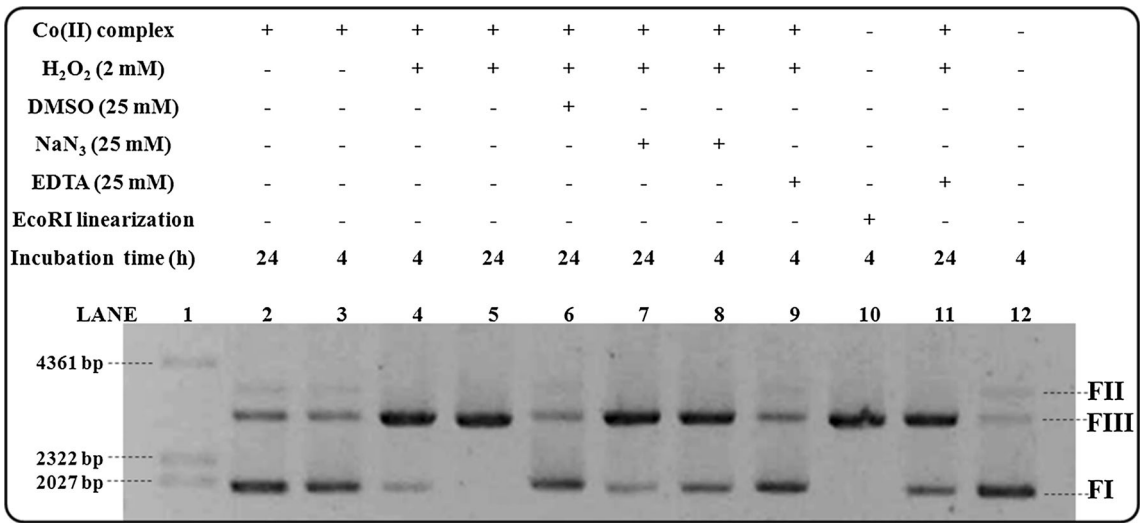

Fig. 8 Agarose gel electrophoresis [0.8 % (w/v)] concerning the incubation of [Co(Cl)(phendione)$_2$(H$_2$O)][BF$_4$] with 200 ng of pBSK II pDNA at pH 7.0 and 37 °C for 4 or 24 h in the absence (*minus signs*) or presence (*plus signs*) of H$_2$O$_2$, reductants, and the chelating agent EDTA, as indicated above each lane. *Lane 1* molecular ladder λDNA/*Hin*dIII, *DMSO* dimethyl sulfoxide, *FI* supercoiled isoform of DNA, *FII* relaxed (nicked) isoform of DNA, *FIII* linear isoform of DNA (double-strand breaks)

[Co(Cl)(phendione)$_2$(H$_2$O)][BF$_4$] and the oxidant may be explained by the equation (L)Co^{2+} + H$_2$O$_2$ → (L)Co^{3+} + OH$^-$ + OH·.

By performing the incubation of pDNA with [Co(Cl)(phendione)$_2$(H$_2$O)][BF$_4$] in the presence of H$_2$O$_2$ and the common hydroxyl radical scavenger DMSO for 24 h, we observed a decrease in pDNA cleavage (Fig. 8, lane 5 vs lane 6), whereas in the presence of NaN$_3$, we observed only a slight decrease [Fig. 8, lanes 8 and 7 vs. lanes 4 and 5 (4 and 24 h, respectively)], indicating a major

contribution from hydroxyl radical in the cleavage process and a minor contribution from superoxide radical. Nevertheless, nuclease activity of [Co(Cl)(phendione)$_2$(H$_2$O)][BF$_4$] is not completely diminished either in the presence of the free-radical scavenger DMSO or in the presence of a singlet-oxygen quencher (NaN$_3$). This means that some pDNA may not be cleaved by an oxidative mechanism, but may possibly be cleaved by a hydrolytic path as observed before for some copper complexes [48]. The incubation of pDNA with [Co(Cl)(phendione)$_2$(H$_2$O)][BF$_4$] for 4 and 24 h in the presence of H$_2$O$_2$ and EDTA, a chelating agent, was also able to decrease the nuclease activity of [Co(Cl)(phendione)$_2$(H$_2$O)][BF$_4$] (Fig. 8, lanes 9 and 11 vs lanes 4 and 5, respectively).

Since the nuclease activity of [Co(Cl)(phendione)$_2$(H$_2$O)][BF$_4$] is not completely diminished in the presence of the free-radical scavenger DMSO or NaN$_3$ (Fig. 8), suggesting that some pDNA may be cleaved by a hydrolytic path, an enzymatic assay was performed using T4 DNA ligase to determine whether the cleaved products induced by [Co(Cl)(phendione)$_2$(H$_2$O)][BF$_4$] were consistent with hydrolysis of the phosphodiester bonds. The efficiency of religation after cleavage by [Co(Cl)(phendione)$_2$(H$_2$O)][BF$_4$] was analyzed (Fig. S4). Despite high levels of pDNA cleavage (Figs. 6, 7, 8), no apparent religation of pDNA was found with [Co(Cl)(phendione)$_2$(H$_2$O)][BF$_4$], indicating that this in vitro cleavage reaction must be operating through some redox chemistry (Fig. S4).

Despite the fact that [Co(Cl)(phendione)$_2$(H$_2$O)][BF$_4$] is capable of in vitro DNA cleavage (Figs. 6, 7, 8) this does not demonstrate the compound displays genotoxic potential ex vivo since it can interact with other biological components before reaching the cell nucleus or, because of its positive charge, may accumulate in other organelles with a negative potential, such as mitochondria [49]. On the other hand, double-strand breaks may result in chromosomal aberrations [50]. In this regard, the induction of chromosomal alterations in the presence of [Co(Cl)(phendione)$_2$(H$_2$O)][BF$_4$] was assessed using Chinese hamster pulmonary fibroblasts (V79) treated with 0.25 μM [Co(Cl)(phendione)$_2$(H$_2$O)][BF$_4$] for 16 h (Fig. 9) or with mitomycin C (positive control). As shown in Fig. 9 no significant alterations in chromosome number or structure were observed in the presence of [Co(Cl)(phendione)$_2$(H$_2$O)][BF$_4$] under the conditions tested. The chromosomal aberrations detected, chromatid breaks and ring chromosomes, accounted together for 4 % of mitotic cells (Fig. 9). In contrast, chromatid and chromosome breaks (28 and 14 %, respectively) and triradial chromosomes (16 %) are the commonest chromosomal alterations found after mitomycin C treatment, accounting for 76 % of aberrant nuclei (Fig. 9). Nevertheless, exposure to

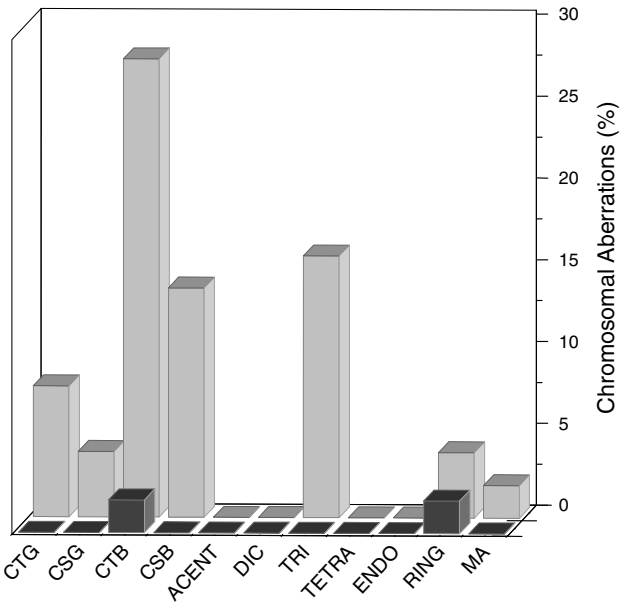

Fig. 9 Induction of chromosomal aberrations in V79 cells by 1.5 μM mitomycin C (*light gray bars*) and 0.20 μM [Co(Cl)(phendione)$_2$(H$_2$O)][BF$_4$] (*dark gray bars*) exposure for 16 h. *CTG* chromatid gap, *CSG* chromosome gap, *CTB* chromatid break, *CSB* chromosome break, *ACENT* acentric chromosome, *DIC* dicentric chromosome, *TRI* triradial chromosome, *TETRA* tetraradial chromosome, *ENDO* endoreduplication, *RING* ring chromosome, *MA* cells with multiple chromosomal aberrations

[Co(Cl)(phendione)$_2$(H$_2$O)][BF$_4$] at concentrations of 0.5 and 1 μM led to a total absence of mitotic cells, and hence no screening for chromosomal aberrations was possible in these conditions (data not shown).

Owing to the lower level of chromosomal aberrations observed in the presence of [Co(Cl)(phendione)$_2$(H$_2$O)][BF$_4$] in V79 cells and so we could analyze further its genotoxic potential, comet assays were performed in HCT116 cells cultivated in the presence or absence of 0.2 μM [Co(Cl)(phendione)$_2$(H$_2$O)][BF$_4$] or H$_2$O$_2$ [0.05 % (v/v)—positive control]. The DNA percentage in the tail was used as a measure for the total DNA strand breakage. Comets were clustered into different classes, according to the observed percentage of DNA in the tail: from class 0 to class 4, corresponding to less than 20 %, 20–40 %, 40–60 %, 60–80 %, and more than 80 % DNA in the tail, respectively. Comets belonging to class 4 (more than 80 % DNA in the tail) were only observed in the positive control [treatment with 0.05 % (v/v) H$_2$O$_2$]. Untreated HCT116 cells showed an average of (12.9 ± 4.0) % DNA in the tail (Fig. S5). Similarly, cells treated with [Co(Cl)(phendione)$_2$(H$_2$O)][BF$_4$] for 12 and 18 h exhibited an average of (11.2 ± 3.4) and (9.3 ± 2.5) % DNA in the tail, respectively (Fig. S5). The average values for the percentage of DNA in the tail show little variation, whether [Co(Cl)(phendione)$_2$(H$_2$O)][BF$_4$]

is present or absent, regardless of the treatment period (12 and 18 h). No significant differences were observed regarding the control ($p < 0.05$) (Fig. S5). Furthermore, no major differences were observed in the comet class distribution (Fig. S5), where comets are normally distributed, with most comets belonging to class 0. These data indicate that [Co(Cl)(phendione)$_2$(H$_2$O)][BF$_4$] does not appear to cause significant genotoxicity in HCT116 cells at the IC$_{50}$. The low genotoxicity exhibited by [Co(Cl)(phendione)$_2$(H$_2$O)][BF$_4$] may be associated with its difficulty in penetrating the nuclear envelope, hindering interactions with DNA [51]. Furthermore, the oxidative stress induced by [Co(Cl)(phendione)$_2$(H$_2$O)][BF$_4$], previously observed by our group through proteomic analysis [27], does not cause ROS-derived genotoxicity as already observed for the chromosomal aberrations (Fig. 9).

As stated above, [Co(Cl)(phendione)$_2$(H$_2$O)][BF$_4$] may also interact with other biological components circulating in the blood plasma of a living organism. HSA is the most abundant protein in plasma, accounting for approximately 60 % of total plasma protein (about 40 mg mL^{-1} or approximately 600 μM) [23]. It consists of a single polypeptide chain with 585 amino acids organized in three domains, and is the major nonspecific transporter protein in blood, with an extraordinary capacity to bind a large variety of both endogenous metabolic compounds and exogenous therapeutic pharmaceuticals [21, 23]. It strongly influences the free drug concentration available—acting as a depot for the therapeutic agent (which may be accessible at higher concentrations than the initial solubility would suggest) or a fast clearance route (preventing the compound from exerting its therapeutic effect when binding is quite strong)—and can, in addition, provide passive targeting owing to the so-called EPR effect [23, 24]. We evaluated the HSA binding of [Co(Cl)(phendione)$_2$(H$_2$O)][BF$_4$] as a first approach to the investigation of its pharmacokinetics as a prospective drug.

Although typically not very informative by itself, UV–vis absorption spectroscopy is a helpful technique as a first approach to the investigation of the interaction between HSA and a metal–ion complex. In this work it was used to access the stability of the complex in aqueous media and to choose the best buffer to study this system, as well as to determine a suitable incubation time for the complex. Time dependence was monitored for 24 h for the complex alone (for stability measurements), and over 48 h at complex-to-HSA molar ratios of 1:1, 1:2, 1:0, and 0:1 .

The stability of [Co(Cl)(phendione)$_2$(H$_2$O)][BF$_4$] was tested at pH 7 in 10 mM Hepes, 10 mM phosphate buffer and 10 mM phosphate buffer with 0.15 M NaCl. Although a variation of approximately 25 % was observed in the intensity of the UV–vis spectra in Hepes buffer, 10 mM phosphate buffer with 0.15 M NaCl was found to be the most suitable for quantitative measurements, with approximately 90 % of the parent complex remaining intact in solution (after a 24 h incubation period at 37.0 ± 0.5 °C). Time dependence measurements for this system showed no changes after a 24-h incubation period (until over 48 h), indicating that this was the most suitable incubation time to ensure that thermodynamic equilibrium conditions were attained (results not shown).

The interaction between [Co(Cl)(phendione)$_2$(H$_2$O)][BF$_4$] and HSA could be detected by UV–vis spectroscopy: there is an approximately 8 % absorbance difference at 259 nm] after 24 h incubation at (37.0 ± 0.5) °C] between the spectra recorded for the sample with a complex-to-HSA molar ratio of 1:1 as compared with the sum of the spectra for the protein alone and the complex alone (at the same concentrations) (Fig. S6). Since the UV–vis spectra for this system did not show significant changes on binding of the complex to the protein, we chose to use fluorescence spectroscopy to assess this interaction.

HSA has 18 tyrosine residues and a single tryptophan residue, Trp214, located in subdomain IIA. This tryptophan residue can be selectively excited at 295 nm, and the corresponding protein emission observed at 340 nm (or longer wavelengths) is quite useful for monitoring the interaction between a compound and HSA. Two major structurally selective binding sites (Sudlow's binding sites I and II) are typically considered for HSA [23]. Trp214 is located within the vicinity of Sudlow's binding site I, but is so

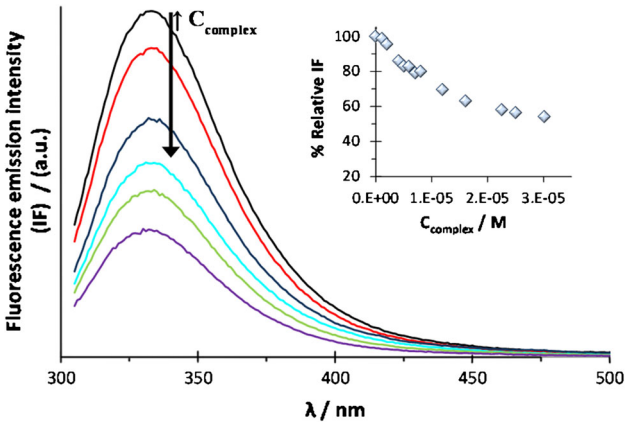

Fig. 10 Steady-state fluorescence data obtained for the binding of [Co(Cl)(phendione)$_2$(H$_2$O)][BF$_4$] to human serum albumin (HSA): Trp214 fluorescence quenching (λ_{exc} = 295 nm) observed on binding of [Co(Cl)(phendione)$_2$(H$_2$O)][BF$_4$] (*black line* HSA alone, *colored lines* samples with increasing concentration of [Co(Cl)(phendione)$_2$(H$_2$O)][BF$_4$] as indicated by the *large arrow*). The *inset* shows the percent relative fluorescence intensity at λ_{em} = 340 nm with increasing concentration of [Co(Cl)(phendione)$_2$(H$_2$O)][BF$_4$]. The conditions were as follows: C_{HSA} = 2.0 μM, kept constant; samples prepared in phosphate buffer pH 7.0/0.15 M NaCl medium; 24 h incubation at (37.0 ± 0.5) °C; measurements at room temperature, (23 ± 1) °C

sensitive to changes in the environment either due to drug binding or due to structural alterations of the protein that it can probe changes occurring in drug binding site II as well. The emission spectra of the protein in the presence of increasing concentrations of [Co(Cl)(phendione)$_2$(H$_2$O)][BF$_4$] are depicted in Fig. 10.

In the absence of [Co(Cl)(phendione)$_2$(H$_2$O)][BF$_4$], the maximum emission intensity for Trp214 is observed at 334 nm (black line in Fig. 10), showing that this residue is protected from the aqueous solvent, where tryptophan would have maximum emission at approximately 350 nm. There is a marked decrease in the Trp214 fluorescence intensity with increasing concentration of [Co(Cl)(phendione)$_2$(H$_2$O)][BF$_4$], reaching approximately 55 % at the highest concentration of [Co(Cl)(phendione)$_2$(H$_2$O)][BF$_4$]. The fluorescence intensity decay with time was measured for all samples, and two illustrative examples (in the absence of [Co(Cl)(phendione)$_2$(H$_2$O)][BF$_4$] and at the highest concentration tested) are presented in Fig. 11, showing that the decay becomes faster (indicating a shorter fluorescence lifetime) in the presence of [Co(Cl)(phendione)$_2$(H$_2$O)][BF$_4$]. [Co(Cl)(phendione)$_2$(H$_2$O)][BF$_4$] thus behaves as a quencher of the Trp214 fluorescence, and the

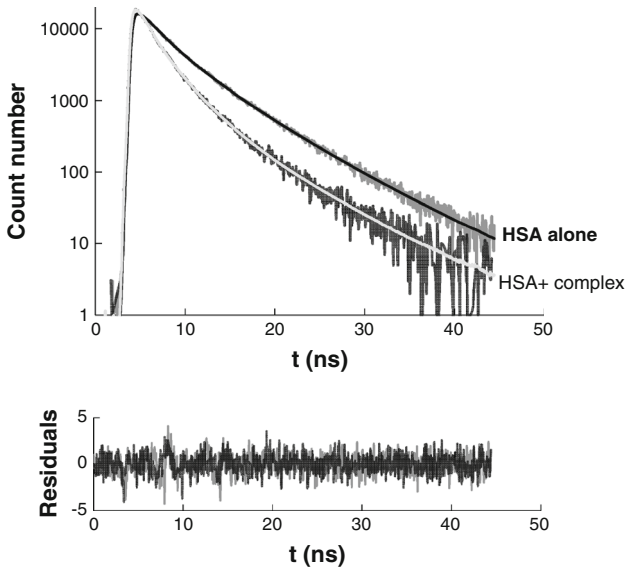

Fig. 11 Fluorescence intensity decay of HSA (Trp214) in the absence (*gray*) and in the presence (*black*) of 30.03 μM [Co(Cl)(phendione)$_2$(H$_2$O)][BF$_4$] measured by the single photon counting technique (see "Materials and methods"). The *lines* are the best fit of a sum of exponentials (Eq. 2) with the following parameters: (1) for HSA alone (*gray line*) $\alpha_1 = \alpha_2 = 0.42$, $\alpha_3 = 0.16$, $\tau_1 = 1.57$ ns, $\tau_2 = 3.70$ ns, $\tau_3 = 6.70$ ns ($\chi^2 = 1.181$); (2) for HSA plus [Co(Cl)(phendione)$_2$(H$_2$O)][BF$_4$] (*black line*): $\alpha_1 = 0.60$, $\alpha_2 = 0.36$, $\alpha_3 = 0.05$, $\tau_1 = 0.87$ ns, $\tau_2 = 2.56$ ns, $\tau_3 = 6.22$ ns ($\chi^2 = 1.184$). The randomly distributed residuals of both fits are shown at the *bottom*. The conditions were as follows: $C_{HSA} = 2.0$ μM, kept constant; samples prepared in phosphate buffer pH 7.0/0.15 M NaCl medium; 24 h incubation at (37.0 ± 0.5) °C; measurements at room temperature, (23 ± 1) °C

nature of this quenching process can be accessed through a Stern–Volmer plot [36, 52].

The Stern–Volmer plots and their detailed analysis are given in Fig. S7. Data analysis shows a 1:1 binding mechanism with a binding constant on the order of log $K_b \sim 4.6$. For a 1:1 binding process, both the steady-state fluorescence intensity (I_F) and the amplitude-weighted mean fluorescence lifetime ($\bar{\tau}$) are a linear combination of the extreme values of those fluorescence spectroscopic variables (denoted below by F) for bound and unbound protein, in which the linear coefficients are the bound and unbound molar fractions:

$$F = \mathcal{X}_{\text{bound}} F_{\text{bound}} + \mathcal{X}_{\text{free}} F_{\text{free}}, \tag{4}$$

which rearranges to

$$\mathcal{X}_{\text{bound}} = \frac{F_{\text{free}} - F}{F_{\text{free}} - F_{\text{bound}}} = \frac{\Delta F}{\Delta F_{\max}}. \tag{5}$$

This is related to the molar concentrations of the species in solution by

$$\begin{aligned} \mathcal{X}_{\text{bound}} &= 1 - \mathcal{X}_{\text{free}} = \frac{[\{\text{HSA} - \text{C}\}]}{[\{\text{HSA}-\text{C}\}] + [\text{HSA}]} \\ &= \frac{[\{\text{HSA} - \text{C}\}]}{C_{\text{HSA}}}, \end{aligned} \tag{6}$$

where HSA denotes the free protein and {HSA–C} denotes the protein–complex adduct, which is in turn related to the association constant:

$$\begin{aligned} K_b &= \frac{[\{\text{HSA}-\text{C}\}]}{[\text{HSA}][\text{C}]} \\ &= \frac{\mathcal{X}_{\text{bound}} C_{\text{HSA}}}{(C_{\text{HSA}} - \mathcal{X}_{\text{bound}} C_{\text{HSA}})(C_{\text{Complex}} - [\{\text{HSA}-\text{C}\}])}, \end{aligned} \tag{7}$$

where the second equality is obtained by using the mass balance for the system and Eq. 6. Using K_b estimated from the Stern–Volmer analysis (Fig. S7) to predict the speciation for the system, we conclude that the following approximation is valid:

$$C_{\text{Complex}} - [\{\text{HSA} - \text{C}\}] \approx C_{\text{Complex}}. \tag{8}$$

Introducing this approximation and rearranging the equation, we obtain the following expression:

$$\mathcal{X}_{\text{bound}} = \frac{\Delta F}{\Delta F_{\max}} = \frac{K_b C_{\text{Complex}}}{1 + K_b C_{\text{Complex}}}. \tag{9}$$

The working equation comes directly from the previous equality:

$$\Delta F = \frac{K_b C_{\text{Complex}}}{1 + K_b C_{\text{Complex}}} \Delta F_{\max}. \tag{10}$$

Thus, representing the experimental ΔF values as a function of the concentration of the complex, and

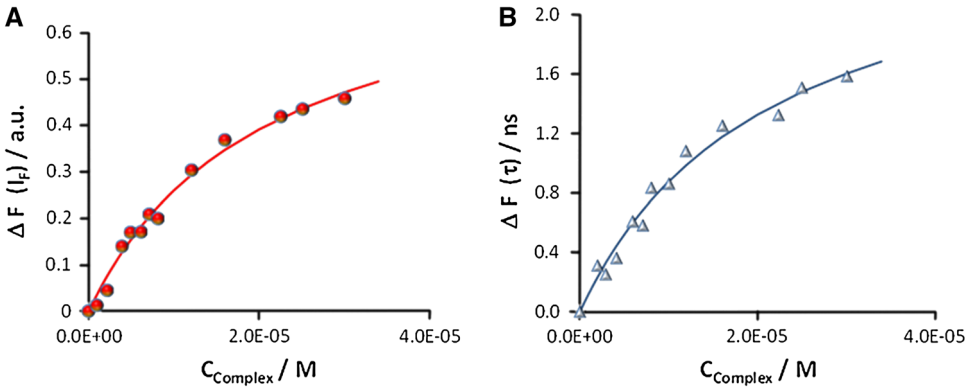

Fig. 12 Variation of fluorescence data obtained for the binding of $[Co(Cl)(phendione)_2(H_2O)][BF_4]$ to HSA with increasing concentration of the complex using Eq. 10. **a** Analysis based on the fluorescence intensity at $\lambda_{em} = 340$ nm ($\lambda_{exc} = 295$ nm) with $\Delta F = (I_F^{free} - I_F^{bound}) = (I_F^{HSA} - I_F)$. **b** Analysis based on the amplitude-weighted fluorescence lifetime with $\Delta F = (\tau^{free} - \tau^{bound}) = (\tau_0 - \tau)$. The conditions were as follow: $C_{HSA} = 2$ μM (constant); $C_{complex} = 0$–30.03 μM in phosphate buffer pH7.0/0.15 M NaCl medium; 24 h incubation at (37 ± 0.5) °C); measurements at room temperature, (23 ± 1) °C

performing a nonlinear fit according to Eq. 10, one retrieves the parameters K_b and ΔF_{max} (Fig. 12). The analysis of the steady-state fluorescence intensity yields log $K_b = 4.69 \pm 0.06$ and that of the fluorescence lifetime yields log $K_b = 4.67 \pm 0.07$. The similarity between the two values supports the binding mechanism proposed, and was anticipated given the parallel trend observed for both I_F and $\bar{\tau}$.

The overlaid trend of the steady-state and time-resolved data (i.e., tending to a plateau for both the amplitude-weighted mean fluorescence lifetime and the steady-state fluorescence intensity) together with the absence of spectral shifts are overall consistent with a mechanism of Förster resonance energy transfer (FRET) being operative [54]. Indeed, the spectral overlap between the HSA Trp214 emission and the absorption of $[Co(Cl)(phendione)_2(H_2O)][BF_4]$ (Fig. S8) makes it possible for radiationless excitation energy transfer from a donor (in this system, HSA Trp214) to an acceptor molecule (in the present case $[Co(Cl)(phendione)_2(H_2O)][BF_4]$) to occur. This quenching mechanism was proposed for the binding of other absorbing species to HSA, such as bilirubin [55] and 4-nitrobenzo-2-oxa-1,3-diazole fluorescent derivatives of bile acids [54] and ruthenium antitumor complexes [53].

FRET efficiency depends on three major factors: (1) the Förster radius R_0, which is the donor–acceptor distance at which there is a 50 % probability of FRET for each excited donor molecule; (2) the donor–acceptor distance within the HSA–complex adduct; (3) the effective fraction of protein bound to the complex. When the protein is saturated with the complex, maximal FRET efficiency is attained, and this can be estimated from ΔF_{max} obtained from the fit of Eq. 10 to the data in Fig. 12 and the value for the same variable in the absence of the complex, i.e., F_{free}:

$$E_{max} = 1 - \frac{F_{bound}}{F_{free}} = \frac{\Delta F_{max}}{F_{free}}. \quad (11)$$

In the present system it was not possible to attain saturation conditions as the absorption and emission inner-filter effect became too high and the fluorescence intensity too low to retrieve reliable experimental values. Nevertheless, the fits of Eq. 10 allowed us to overcome this experimental limitation. The FRET efficiencies thereby obtained are 79.4 and 83.0 % for the steady-state intensity and the lifetime data, respectively. These two values are in excellent agreement. It is possible now to calculate the distance between the complex and HSA Trp214 once the Förster radius R_0 is known. This critical distance (R_0) can be computed from spectroscopic data [56], and the details of the calculation are given in Fig. S7. The value obtained for R_0 in the FRET process HSA Trp214 → complex was (19 ± 1) Å. The donor–acceptor distance, R, is then calculated from

$$R = (1/E - 1)^{1/6} R_0. \quad (12)$$

Taking into account the values of R_0 and the FRET efficiency mentioned previously, we estimate the donor–acceptor distance, i.e., the Trp214–complex spatial separation, to be 15 ± 1 Å.

These fluorescence spectroscopic studies, based on Trp214 emission, do not rule out completely the existence of another binding site at a distance from Trp214 that would not influence its fluorescence properties, or some other nonspecific interaction within a region of the protein well separated from Trp214. However, these hypotheses are highly unlikely since the nonspecific adsorption would lead to structural alterations undoubtedly sensed by Trp214, and also because it would (at least in part) occur near its indole group, thereby quenching its fluorescence.

The existence of another binding site with an association constant of the same magnitude as or greater than that calculated here would also influence the trend of the observed fluorescence quenching because the availability of the complex for binding near Trp214 would also depend on that other hypothetical constant. This would result in a more complex behavior than the one observed in Fig. 12, which is close to linear for low concentrations of the complex and with a negative curvature well described by a simple quadratic equation for high complex-to-protein molar ratios, and afterwards shown to be very well described by a simple 1:1 binding model.

To summarize, our fluorescence spectroscopy studies thus indicate that there is a moderate and specific interaction of $[Co(Cl)(phendione)_2(H_2O)][BF_4]$ with HSA, involving one binding site, at a distance of approximately 1.5 nm for the Trp214 indole side chain with log $K_b \sim 4.7$. This binding constant is of the same order of magnitude as that obtained for KP1019, a ruthenium anticancer complex currently in phase II clinical trials known to bind reversibly to HSA and for which log $K = 4.025$ was reported [21].

Our results thus suggest that $[Co(Cl)(phendione)_2(H_2O)][BF_4]$ can be efficiently transported by albumin in the blood plasma. This reversible HSA interaction, which can improve the delivery of $[Co(Cl)(phendione)_2(H_2O)][BF_4]$ to tumor cells on the basis of the passive targeting associated with the EPR effect, together with the observed in vitro antiproliferative effect is a very promising feature regarding the in vivo effect of $[Co(Cl)(phendione)_2(H_2O)][BF_4]$.

Concluding remarks

The results presented here enabled us to further confirm (1) the in vitro antiproliferative potential of $[Co(Cl)(phendione)_2(H_2O)][BF_4]$ with regard to tumor cells by showing lower cytotoxicity against nontumorigenic epithelial mammary gland cells compared with our previous results in tumor cell lines [26] and (2) the activation of the expression of apoptotic genes and the ability of UDCA to reduce cell death. However, apoptosis may not result from complex-induced DNA damage as our results clearly indicate that the compound does not exert any significant clastogenic effect. We reported an affinity constant for CT-DNA that is roughly half that determined for the known DNA-interacting antitumor agent doxorubicin under the same test conditions. Also, $[Co(Cl)(phendione)_2(H_2O)][BF_4]$ demonstrates the ability to act as a double-strand cleaving agent in a concentration-dependent fashion by a mechanism that must be operating through some redox chemistry.

A specific interaction with HSA was observed by fluorescence spectroscopy, indicating the existence of one binding site at a distance estimated as approximately 1.5 nm for the Trp214 indole side chain. The moderate HSA binding constant of log $K_b = 4.68 \pm 0.09$ indicates that $[Co(Cl)(phendione)_2(H_2O)][BF_4]$ can be efficiently transported in the bloodstream by albumin. This reversible HSA interaction, which can improve the delivery of $[Co(Cl)(phendione)_2(H_2O)][BF_4]$ to tumor cells on the basis of the passive targeting associated with the EPR effect, together with the observed in vitro antiproliferative effect is a very promising feature regarding the in vivo effect of $[Co(Cl)(phendione)_2(H_2O)][BF_4]$. Our group will test this hypothesis by evaluating the ability of the free complex to decrease tumor volume in a mouse model. Additionally, active targeting strategies will also be developed, namely, the use of nanoparticles to further target $[Co(Cl)(phendione)_2(H_2O)][BF_4]$ to tumor cells. Particularly, these interesting results obtained for the interaction of $[Co(Cl)(phendione)_2(H_2O)][BF_4]$ with HSA are also suggestive that albumin nanoparticles may prove to be useful delivery systems for $[Co(Cl)(phendione)_2(H_2O)][BF_4]$, improving the in vivo biodistribution and consequently its cytotoxicity and efficacy as an antitumor drug.

Additionally, the results presented here are very useful for future design of a delivery system, as the excellent complex–HSA interaction observed suggests that albumin nanoparticles may be used as effective nanocarriers for this phendione compound.

Acknowledgments Part of this work was financed by Portuguese national funds through FCT, the Portuguese Foundation for Science and Technology, within the scope of projects PTDC/QuiQui/101187/2008, PEst-OE/QUI/UI0612/2013, and PEst-OE/QUI/UI0536/2013, as well as Ciência2008 and Investigator FCT-POPH initiatives. We thank Ana C. Silva for fruitful discussions.

References

1. Hannon MJ (2007) Pure Appl Chem 2243–2261
2. Meggers E (2009) Chem Commun 1001–1010. doi:10.1039/b813568a
3. Zhang CX, Lippard SJ (2003) Curr Opin Chem Biol 7:481–489
4. Cantero G, Pastor N, Mateos S, Campanella C, Cortes F (2006) Mutat Res 599:160–166. doi:10.1016/j.mrfmmm.2006.02.006
5. Zeglis BM, Pierre VC, Barton JK (2007) Chem Commun 4565–4579. doi:10.1039/b710949k
6. Williams NH, Takasaki B, Wall M, Chin J (1999) Acc Chem Res 32:485–493
7. Jiang Q, Xiao N, Shi PF, Zhu YG, Guo ZJ (2007) Coord Chem Rev 251:1951–1972. doi:10.1016/j.ccr.2007.02.013
8. Pasini A, Zunino F (1987) Angew Chem Int Ed Engl 26:615–624. doi:10.1002/anie.198706151
9. Barton JK (1986) Science 233:727–734

10. Wang J, Cai X, Rivas G, Shiraishi H, Farias PA, Dontha N (1996) Anal Chem 68:2629–2634
11. Wheate NJ, Brodie CR, Collins JG, Kemp S, Aldrich-Wright JR (2007) Mini Rev Med Chem 7(6):627–648
12. Cusumano M, Di Pietro ML, Giannetto A (2006) Inorg Chem 45:230–235. doi:10.1021/ic050880o
13. Liu HK, Sadler PJ (2011) Acc Chem Res 44(5):349–359. doi:10.1021/ar100140e
14. Dhar S, Senapati D, Das PK, Chattopadhyay P, Nethaji M, Chakravarty AR (2003) J Am Chem Soc 125:12118–12124. doi:10.1021/ja036681q
15. Patra AK, Dhar S, Nethaji M, Chakravarty AR (2003) Chem Commun 1562–1563
16. Reddy PA, Santra BK, Nethaji M, Chakravarty AR (2004) J Inorg Biochem 98:377–386
17. Ranford JD, Sadler PJ, Tocher DA (1993) J Chem Soc Dalton Trans 3393–3399. doi:10.1039/DT9930003393
18. Bruijnincx PC, Sadler PJ (2008) Curr Opin Chem Biol 12:197–206. doi:10.1016/j.cbpa.2007.11.013
19. Gabbiani C (2009) Proteins as possible targets for antitumor metal complexes. Biophysical studies of their interactions. Firenze University Press, Florence
20. Hernandes MZ, Pontes FJ de S, Coelho LCD, Moreira DRM, Pereira VRA, Leite ACL (2010) Curr Med Chem 17:3739–3750
21. Pessoa JC, Tomaz I (2010) Curr Med Chem 17:3701–3738
22. US Food and Drug Administration (2006) Requirements on content and format of labeling for human prescription drug and biological products, section 12: clinical pharmacology, subsection 12.3: pharmacokinetics, p 262. http://www.fda.gov/OHRMS/DOCKETS/98fr/00n-1269-nfr0001-03.pdf
23. Colmenarejo G (2003) Med Res Rev 23:275–301. doi:10.1002/med.10039
24. Kratz F (2008) J Control Release 132:171–183. doi:10.1016/j.jconrel.2008.05.010
25. Maeda H (2010) Bioconjug Chem 21:797–802. doi:10.1021/bc100070g
26. Silva TFS, Smoleński P, Martins LMDRS, Guedes da Silva MFC, Fernandes AR, Luis D, Silva A, Santos S, Borralho PM, Rodrigues CMP, Pombeiro AJL (2013) Eur J Inorg Chem 2013:3651–3658. doi:10.1002/ejic.201300197
27. Silva A, Luis D, Santos S, Silva J, Mendo AS, Coito L, Silva TF, da Silva MF, Martins LM, Pombeiro AJ, Borralho PM, Rodrigues CM, Cabral MG, Videira PA, Monteiro C, Fernandes AR (2013) Drug Metab Drug Interact 28:167–176. doi:10.1515/dmdi-2013-0015
28. Heintz RA, Smith JA, Szalay PS, Weisgerber A, Dunbar KR (2002) In: Coucouvanis D (ed) Inorganic synthesis, vol 33. Wiley, New York, pp 75–107
29. Silva TFS, Martins LMDRS, Guedes da Silva MFC, Fernandes AR, Silva A, Borralho PM, Santos S, Rodrigues CMP, Pombeiro AJL (2012) Dalton Trans 41:12888–12897. doi:10.1039/C2DT11577H
30. Schmittgen TD, Livak KJ (2008) Nat Protoc 3:1101–1108
31. Li Y, Liu J, Li Q (2010) Mol Carcinog 49:566–581. doi:10.1002/mc.20623
32. Rahman KW, Li Y, Wang Z, Sarkar SH, Sarkar FH (2006) Cancer Res 66:4952–4960. doi:10.1158/0008-5472.CAN-05-3918
33. Kanakis CD, Tarantilis PA, Polissiou MG, Diamantoglou S, Tajmir-Riahi HA (2007) Cell Biochem Biophys 49:29–36
34. Conde J, Larguinho M, Cordeiro A, Raposo LR, Costa PM, Santos S, Diniz MS, Fernandes AR, Baptista PV (2014) Nanotoxicology 8:521–532
35. Jakusch T, Hollender D, Enyedy EA, Gonzalez CS, Montes-Bayon M, Sanz-Medel A, Costa Pessoa J, Tomaz I, Kiss T (2009) Dalton Trans 2428–2437. doi:10.1039/B817748A
36. Valeur B (2001) Molecular fluorescence. Wiley-VCH, Weinheim, pp 155–199
37. Hampton MB, Orrenius S (1997) FEBS Lett 414:552–556
38. Dosa PI, Ward T, Castro RE, Rodrigues CM, Steer CJ (2013) ChemMedChem 8:1002–1011. doi:10.1002/cmdc.201300059
39. Takaki K, Higuchi Y, Hashii M, Ogino C, Shimizu N (2013) J Biosci Bioeng. doi:10.1016/j.jbiosc.2013.06.003
40. Tang HL, Yuen KL, Tang HM, Fung MC (2009) Br J Cancer 100:118–122. doi:10.1038/sj.bjc.6604802
41. Xie X, Wang S, Wong TC, Fung M (2013) Cancer Cell Int 13:63
42. Amaral JD, Castro RE, Steer CJ, Rodrigues CM (2009) Trends Mol Med 15:531–541. doi:10.1016/j.molmed.2009.09.005
43. Amaral JD, Castro RE, Sola S, Steer CJ, Rodrigues CM (2007) J Biol Chem 282:34250–34259. doi:10.1074/jbc.M704075200
44. Taguchi T, Kato Y, Baba Y, Nishimura G, Tanigaki Y, Horiuchi C, Mochimatsu I, Tsukuda M (2004) Oncol Rep 11:421–426
45. Gartel AL, Tyner AL (2002) Mol Cancer Ther 1:639–649
46. Ramakrishnan S, Suresh E, Riyasdeen A, Akbarsha MA, Palaniandavar M (2011) Dalton Trans 40:3245–3256. doi:10.1039/c0dt01360a
47. Karidi K, Garoufis A, Tsipis A, Hadjiliadis N, den Dulk H, Reedijk J (2005) Dalton Trans 1176–1187. doi:10.1039/b418838a4
48. Babu MSS, Reddy KH, Krishna PG (2007) Polyhedron 26:572–580. doi:10.1016/j.poly.2006.08.026
49. Modica-Napolitano JS, Aprille JR (2001) Adv Drug Deliv Rev 49:63–70
50. Obe G, Johannes C, Ritter S (2010) Mutat Res 701:3–11. doi:10.1016/j.mrgentox.2010.05.010
51. Jung Y, Lippard J (2007) Chem Rev 107:1387–1407
52. Matos CP, Valente A, Marques F, Adão P, Paula Robalo M, de Almeida RFM, Pessoa JC, Santos I, Helena Garcia M, Tomaz AI (2013) Inorg Chim Acta 394:616–626. doi:10.1016/j.ica.2012.09.026
53. Demoro B, de Almeida RFM, Marques F, Matos CP, Otero L, Costa Pessoa J, Santos I, Rodriguez A, Moreno V, Lorenzo J, Gambino D, Tomaz AI (2013) Dalton Trans 42:7131–7146. doi:10.1039/C3DT00028A
54. Rohacova J, Marin ML, Miranda MA (2010) J Phys Chem B 114:4710–4716. doi:10.1021/jp911114n
55. Honore B, Pedersen AO (1989) Biochem J 258:199–204
56. Loura LM, de Almeida RF, Coutinho A, Prieto M (2003) Chem Phys Lipids 122:77–96